Volume 16, Number 3, 2023. pp. 305-320

Jordan Journal of Physics

ARTICLE

Investigation of the Effect of Deposition Time and Annealing on the Structural and Optical Properties of Chemically Deposited ZnS Thin Films

Oluwatoyin Osanyinlusi[a], Anthony I. Mukolu[b], Aderemi B. Alabi[a], Muyiwa M. Orosun[a], Mufutau A. Salawu[a], Kamaldeen A. Yusuf[a] and Adebayo. A. Adeyinka[a]

[a] *Department of Physics, Faculty of Physical Sciences, University of Ilorin, Ilorin, Kwara State, Nigeria.*

[b] *Department of Physics, Faculty of Science, Ekiti State University, Ado Ekiti, Ekiti State, Nigeria.*

Doi: https://doi.org/10.47011/16.3.6

Received on: 21/09/2021; Accepted on: 28/11/2021

Abstract: The Chemical bath deposition (CBD) technique was successfully used to deposit ZnS thin films. The effects of deposition time and annealing on the structural and optical properties of the obtained thin films were investigated by X-ray diffraction (XRD), and UV-Vis spectrophotometer, respectively. The XRD pattern for the as-deposited ZnS thin films deposited for 30 min showed three peaks at 2θ values of 28.75°, 48.05°, and 56.47° corresponding to (111) (main peak), (220), and (311) reflection planes, indicating cubic structure. Comparing these peaks with that of the films prepared for 60 min, the latter have narrower widths, are more intense, sharper, and produce another weak peak at 2θ angle of 33.51°. Post-annealing treatment results in even more intense and sharper peaks, with their width narrowing further, causing an improvement in the crystallinity. The grains detected from the SEM micrograph are well-defined with spherical shapes of varying sizes. The grain shape changes after annealing due to coalescence of the grains. According to the EDX result, Zn and S were present in the prepared film. The as-deposited films showed a maximum transmittance of 82.1% at the visible region, which increased to 89.2% after annealing. The optical energy band gap was found to be in the ranges of 3.58 - 3.75 eV and 3.41 - 3.73 eV for the as-deposited and annealed films, respectively, signifying that the energy band gap decreases with annealing.

Keywords: Chemical bath deposition, Zinc sulphide, Optical properties, Annealing, Thin films, Deposition time.

1. Introduction

Cost reduction as well as improvement in efficiency has always been the concern of optoelectronic devices research [1], and in recent years most material science studies have been focusing on wide band gap compound semiconductor materials. One example of such materials is zinc sulphide (ZnS), which is an n-type II–VI compound semiconductor with a direct and wide band gap (3.5–3.7 eV) at room temperature. It belongs to the metal chalcogenide compound group and crystallizes in both cubic and hexagonal forms [2].

Furthermore, ZnS has been reported to have a high refractive index and dielectric constant, with values of 2.35 at 632 nm and 9 at 1 MHz, respectively [3]. Additionally, ZnS exhibits transparency to visible radiation while remaining opaque to ultraviolet and near-infrared radiations

Corresponding Author: Oluwatoyin Osanyinlusi **Email**: osanyinlusi.o@unilorin.edu.ng

[4, 5]. As a result, it has been extensively studied for its uses in various application devices such as blue light-emitting diodes, flat panel displays, sensors, lasers, reflectors, planar waveguides, and n-type window layers for thin film heterojunction solar cells [6, 7]. Due to its superior chemical stability in comparison to other chalcogenides, ZnS has also been used as an important phosphor for photoluminescence (PL), electroluminescence (EL), and cathodoluminescence (CL) devices [8]. Thin film devices have become the primary focus of research in the field of science and technology because of their distinctive and novel properties [9].

CdS thin films have recently been adjudged as the most efficient window layer in thin film heterojunction solar cells because of their superior electrical performances and simplicity in preparation [10]. However, the high toxicity of cadmium presents a substantial environmental concern, primarily due to the waste production generated during the CdS fabrication [10]. Furthermore, because of its low band gap (2.42 eV), CdS is known to absorb the blue region of the solar spectrum which leads to a decrease in the short circuit current of the solar cells [11]. As a result of these shortcomings, ZnS thin films have been suggested as a preferred alternative for window layers in thin film heterojunction solar cells because of their non-toxicity and higher band gap [9, 12]. A higher band gap facilitates the transmission of high-energy photons to the junction, eliminating absorption losses and enhancing the blue response of devices. Thus, the overall solar cell power conversion efficiency is increased [13].

Recently, ZnS thin films have been successfully used as a replacement for CdS in CIGS-based solar cells and have achieved a maximum efficiency of 18.6% [14]. Research has shown that the properties of thin films depend to a large extent on the technique of deposition [15]. Different techniques have been successfully used in the fabrication of ZnS thin films, including sputtering [10], molecular beam epitaxy [16], pulsed laser deposition [17], electrodeposition [18], chemical vapor deposition [19], successive ionic layer adsorption and reaction [20], spray pyrolysis [12, 21], and chemical bath deposition (CBD) [3, 22].

Among these methods, CBD is the most attractive as a large-area growth technique, because it is free of vapor deposition associated with other high-temperature fabrication techniques [23]. CBD has become a common deposition technique for some metal chalcogenides, such as sulfides and selenides of zinc (Zn), cadmium (Cd), and lead (Pb) [24].

In the process of metal chalcogenide thin films deposition using the CBD technique, the substrates are vertically immersed in diluted metal ion-containing solutions with the selected chalcogenide precursors. The introduction of an appropriate complexing agent regulates the hydrolysis of the metal ion and provides some stability to the bath. This addition accelerates the hydrolysis and precipitation processes. Under these conditions, the procedure involves the slow release of chalcogen ions into the solution in which the free metal ion is buffered at a low concentration. Thin film formation on the substrate takes place when the ionic product (IP) exceeds the solubility product (SP) [25]. A soluble salt containing Zn ion and an S source compound dissolved in an aqueous solution are required for the deposition of ZnS thin films using the CBD technique. These components react according to the following equation: Zn^{2+}+ $S^{2-} \rightarrow$ ZnS. The solubility product value for this reaction at 25ºC is reported to be $K_{sp} = 10^{-24.7}$ [26].

Usually, a post-annealing treatment is required during the fabrication of thin films to improve the quality of the crystal or stabilize the structure at a particular temperature [27].

Chemical deposition of ZnS thin films has been grown in an aqueous alkaline bath by many authors [28, 29]. Manjulavalli and Kannan [28] used zinc acetate and thiourea as zinc and sulphur sources, respectively, with ammonia as the complexing agent. They prepared ZnS thin films with varied molar concentrations of zinc acetate and reported that the optical band gap energy decreased from 3.96 to 3.84 eV with increasing molar concentration from 0.5 to 2 M. Erken *et al*. [29] studied the effects of deposition time on the optical and electrical properties of ZnS semiconductor thin films using CBD technique. The ZnS was deposited over varying durations, ranging from 4 to 8 hours, in a reaction bath containing mixtures of $ZnSO_4$, NH_3, $CS(NH_2)_2$ (thiourea), and $N(CH_2CH_2OH)_3$ (TEA) at 80ºC. The prepared ZnS thin films had

a maximum transmittance of 90% and a range of energy band gap between 3.61 and 3.88 eV, which increased with extending the deposition time.

In the present study, ZnS thin films with different thicknesses were grown by the CBD technique by varying the deposition times. The prepared films were annealed in air at 673 K and analyzed for their structural, morphological, and optical properties by using X-ray diffraction (XRD), scanning electron microscopy (SEM), and optical absorption studies.

2. Experimental Methods

The chemical bath deposition (CBD) technique was used in the deposition of ZnS films onto a glass substrate following an earlier reported procedure [30]. Commercially available glass slides of dimensions 26 × 76 × 2 mm were used as the substrate. Since substrate cleaning plays an important role in the deposition of thin films, the slides were ultrasonically cleaned in methanol, acetone, and distilled water successively. Zinc sulphate heptahydrate ($ZnSO_4.7H_2O$) (BDH) was used as the zinc ion source and $CS(NH_2)_2$ (thiourea) (Sigma Aldrich) as the sulphide ion source. Ammonia (NH_3) (BDH) was used as the complexing agent. All chemicals were of analytical grade and used as received without any further purification. For the preparation of ZnS thin films, 50 ml 0.2 M zinc sulfate solution was prepared in a 100 ml beaker using distilled water and this solution was stirred with a magnet stirrer for 30 minutes. Ammonia was added dropwise to the $ZnSO_4$ solution as a complexing agent. Initially, the solution turned milky, but it became clear and transparent upon the addition of excess ammonia. The pH was stabilized at 10.9 during the process. The mixture was continuously stirred for 60 minutes at 343 K using a hotplate stirrer. An equal volume of 0.2 M thiourea solution, prepared using distilled water, was added drop by drop to the previously prepared bath containing $ZnSO_4$ and NH_3, with continuous stirring. After 60 minutes of stirring at the temperature of 343 K, the treated glass slides were vertically inserted into the prepared chemical bath solution. The glass slides were sequentially removed from the beaker after the periods of 30, 45, and 60 min, and they were cleaned with distilled water in order to remove the loosely adherent white powders precipitates that had formed in the solution during deposition. The obtained films were white, uniform, and with a good adherence to the substrate. The thickness of the prepared ZnS thin films was determined by the weight difference method. Each prepared sample was cut into two parts with one part annealed in air at 673 K for one hour using a Carbolite furnace. The structural characterization of the films was carried out by X-ray diffraction technique using an X-ray diffractometer (Rigaku D/Max - lllC) with CuKα radiation (α =1.5404Å) at 40 kV and 20 mA. The SEM images and elemental compositions of the ZnS were analyzed using Scanning Electron Microscopy coupled with an energy dispersion X-ray (EDX) spectrometer (JEOL JSM 7600F Field emission SEM). The optical transmittance was recorded using the Avantes-SAI-07086751 model UV-V spectrophotometer in the range of 300-1000 nm. The spectral data was used to determine the extinction coefficient, skin depth, dielectric constants, and the band gap present in the samples. The Fourier Transform infrared spectrophotometer (FT-IR) analysis was taken by Nicolet iS10 FT-IR spectrometer.

3. Results and Discussion

3.1 Reaction Mechanism

The chemical reaction mechanism for the formation of ZnS films is proposed as follows [31]:

(1) Controlling the Zn^{2+} concentration using ammonia

$$Zn^{2+} + 4NH_3 \leftrightarrow Zn(NH_3)_4^{2+} \quad (1)$$

(2) Hydrolysis of thiourea in an alkaline medium to produce S^{2-}

$$SC(NH_2)_2 + 2OH^- \leftrightarrow S^{2-} + H_2NCN + 2H_2O \quad (2)$$

(3) Formation of ZnS films:

$$Zn(NH_3)_4^{2+} + S^{2-} \leftrightarrow ZnS + 4NH_3 \quad (3)$$

When the unbound Zn^{2+} and S^{2-} exceed the solubility product of ZnS, the precipitation of ZnS can occur either in solution or on the surface of the substrates:

$$Zn^{2+} + S^{2-} \leftrightarrow ZnS \quad (4)$$

The formation of ZnS can be generally summarized as thus:

$$Zn(NH_3)_4^{2+} + (NH_2)_2CS + 2OH^- \rightarrow ZnS + CH_2N_2 + 4HN_3 + 2H_2 \quad (5)$$

3.2 Thickness Measurement

The thicknesses of ZnS films deposited for 30, 45, and 60 min were calculated using the gravimetric analysis represented by Eq. (6) [29]. The method involves weighing the glass slide substrate before (m_1) and after the film deposition (m_2), with the density of the coated substance used for the determination of the average thickness (t) of the films.

$$t = \frac{\Delta m}{A * \rho} \quad (6)$$

where $\Delta m = m_2 - m_1$ is the mass difference in grams, ρ is the density of ZnS in g/cm^3 , and A is the area of the deposition surface in cm^2. It is considered that the film is uniform for the entire sample, and a constant density value of ZnS is taken as 4.09 g/cm^3. The thicknesses were calculated as 72, 125, and 150 nm for the thin films deposited for 30, 45, and 60 min, respectively. The variation of thickness with deposition time is presented in Fig.1 where it can be observed that the thickness of the film increases with increasing deposition time.

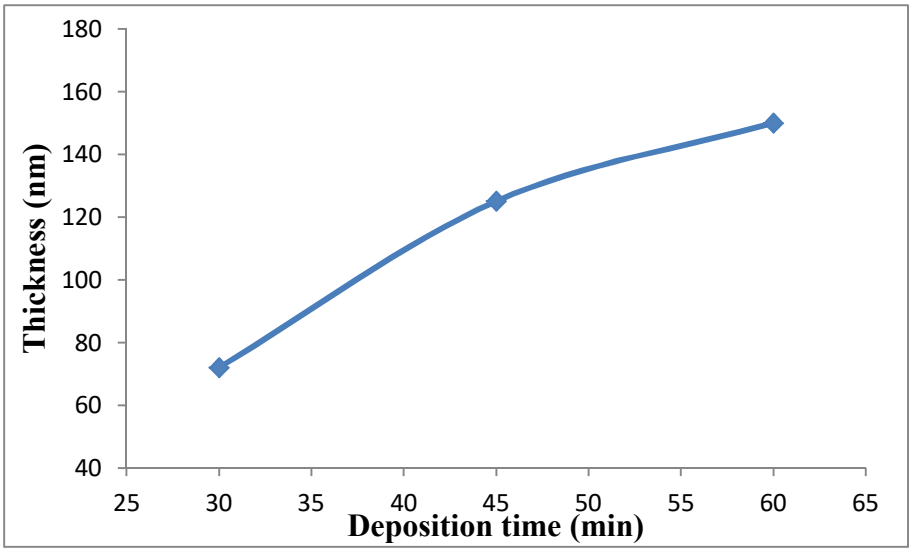

FIG. 1. Variation of thickness with deposition time.

3.3 Morphology

Figures 2(a) and 2(b) show the surface morphology for as-deposited and annealed ZnS thin films prepared for 60 min as recorded by SEM (Scanning Electron Microscope). The micrographs reveal that the deposited films show uniformity across their entirety, displaying no voids or cracks and effectively covering the substrates. As seen in Fig. 2 (a), the as-deposited film morphology shows well-defined spherical-shaped grains of different sizes. However, upon annealing the film in air at 673 K, as depicted in Fig. 2(b), the spherical shape of the grains changes with the surface becoming smooth. This may be due to the agglomeration of smaller particles leading to the disappearance of the grain boundaries after annealing [32].

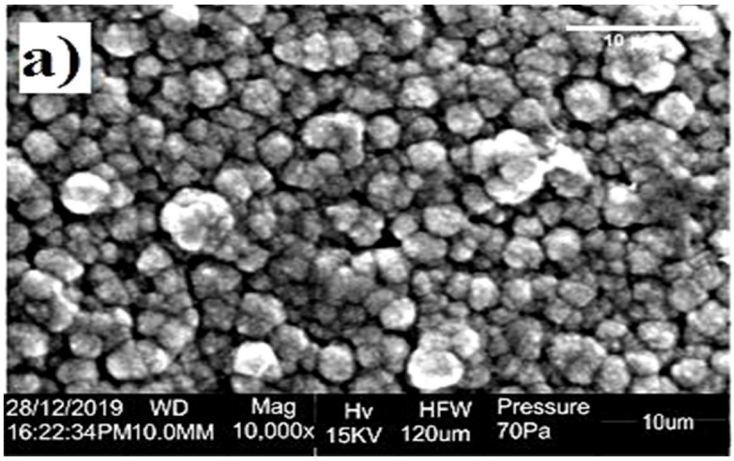

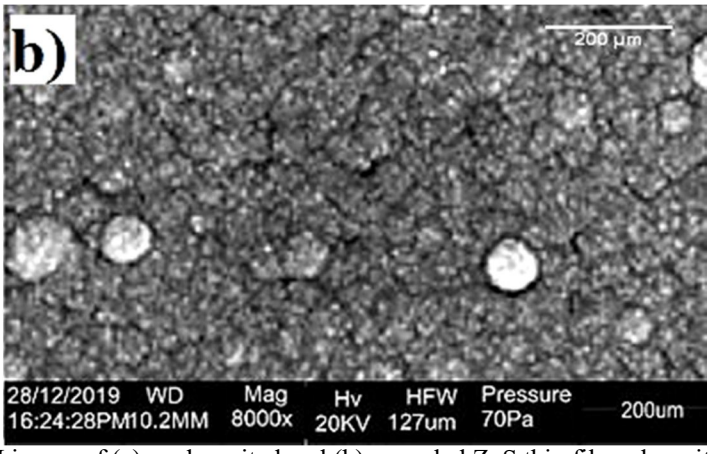

FIG. 2. SEM image of (a) as-deposited and (b) annealed ZnS thin films deposited at 60 min

3.4 Elemental Analysis

Typical EDX analysis was carried out for the as-deposited film deposited for 60 min in order to identify the constituents of the prepared samples, and the result of the analysis is shown in Fig. 3. The analysis confirms the presence of Zn and S in the film and reveals that the prepared ZnS films are non-stoichiometry with atomic percentage S/Zn ratio of 0.58, which shows that the percentage of sulphur is low, indicating sulphur deficiency in the films. This deficiency of sulphur may be attributed to its volatility and its affinity towards oxygen. Consequently, it could have either evaporated or been converted to SO_2 before evaporating [33]. The peak associated with oxygen (O) could originate from the surrounding atmospheric air or the aqueous nature of the bath solution. Furthermore, considering that the chemical bath is prepared with the solution's pH maintained in an alkaline condition, the presence of hydroxide ions (OH^-) would likely have a significant impact on the deposition process. This influence would promote the incorporation of oxygen into the deposited films, leading to a higher level of oxygen contamination. Nakada *et al.* [34] reported that the introduction of an oxygen atom into his chemically deposited ZnS film may be a result of the production of ZnO or $Zn(OH)_2$ in the reaction bath during the deposition of ZnS thin films. Also, Kalyanasundaram *et al*. [35] suggested that the presence of oxygen in ZnS film might have been due to the glass substrate. The excess zinc in the film may be attributed to the production of ZnO or $Zn(OH)_2$ resulting from the alkaline reaction solution [36]. Carbon (C) might have been incorporated into the ZnS films from the initial precursor of thiourea [37]. A similar result has been reported by Choudapur *et al*. [38].

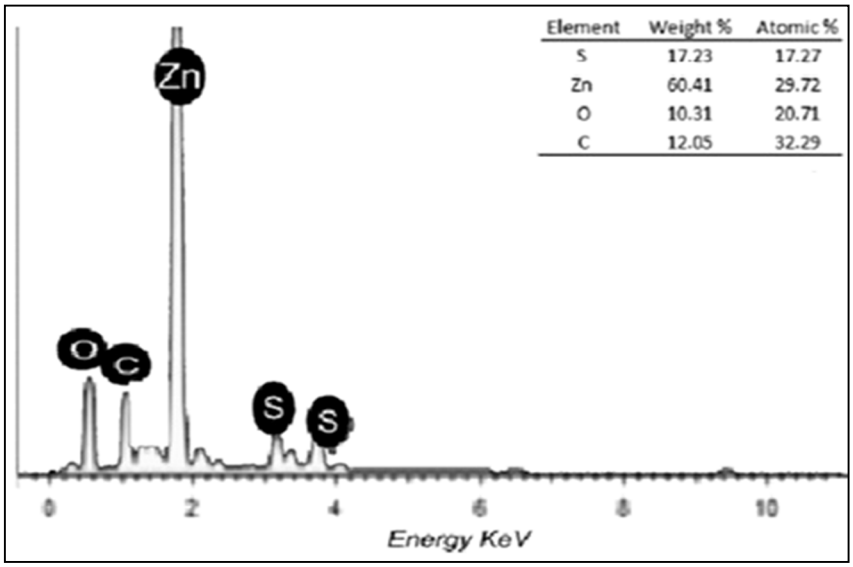

FIG. 3. EDX image for as-deposited ZnS prepared for 60 min.

3.5 Structural Analysis

Figure 4 shows the XRD pattern of the as-deposited ZnS thin film sample deposited for 30 min. Three intense diffraction peaks were observed, located at 2θ values of 28.75°, 48.05°, and 56.47° and indexed as (111), (220), and (311) reflections of cubic ZnS, respectively, with a strong preferred orientation along the (111) plane. This is in good agreement with the standard JCPDS card No.05-0566 [38]. ZnS thin film grown by CBD, with a cubic structure, has been previously reported by Nabiyouni *et al.* [39]. Figure 5 on the other hand, shows the structural pattern of as-deposited and annealed ZnS thin films deposited for 60 min. In the as-deposited film, as evident from Fig. 5(a), the intensity of the peaks increases while the peaks themselves become narrower, as compared to the film deposited for 30 min. This finding indicates that with increasing deposition time the degree of crystallinity of the film increases. Emergence of one other weak peak (200) at 2θ angle value 33.51° of a cubic phase was also observed.

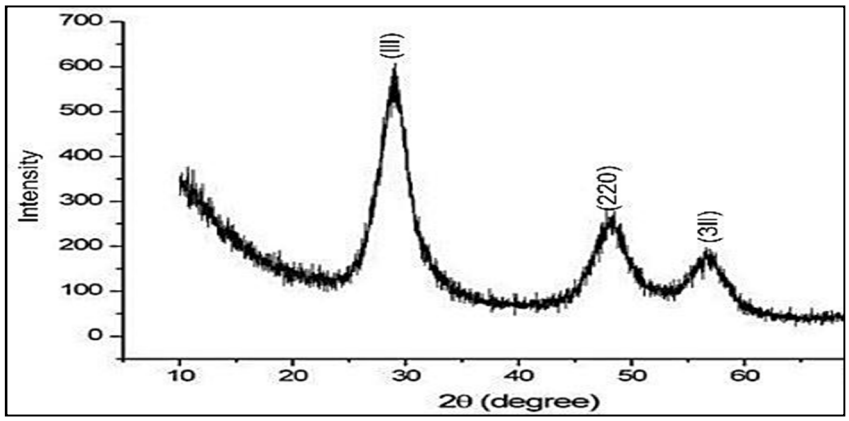

FIG. 4. X-ray diffraction patterns for as-deposited ZnS thin films deposited for 30 min.

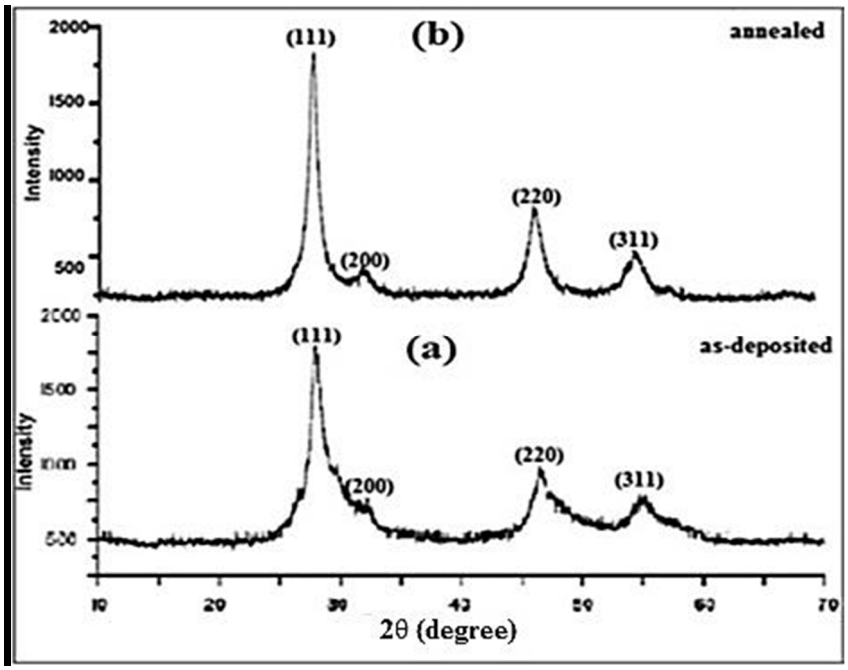

FIG. 5. X-ray diffraction patterns for as-deposited and annealed ZnS thin films deposited for 60 min.

As shown in Fig. 5(b), when the film deposited for 60 min is subjected to post-annealing treatment at 673 K in air for one hour, the overall intensity of all the peaks becomes more intense and sharper, with further narrowing of the peaks' width, indicating a further increase in their crystalline nature [40, 41]. These behaviour are likely because of the reduced strain within the film due to some degree of reorientation of the particles at higher temperatures [42, 43].

The mean crystallite sizes (D) of the films are calculated using the Scherrer formula [44]

$$D = \frac{K\lambda}{\beta os\theta} \quad (7)$$

where K is a dimensionless constant whose value is approximately 0.94, λ is the wavelength of the X-ray used (1.5406Å), β is the full width half maximum (FWHM) of the most intense peak (in radians), and θ is the Bragg's angle.

The micro-strain (ε) developed in the thin films is calculated from the relation [45].

$$\varepsilon = \frac{\beta cos\theta}{4} \quad (8)$$

where θ is Bragg's angle, β is the width at half of the maximum peaks.

A dislocation is a crystal defect or irregularity that occurs within a crystal structure [46]. The dislocation density (δ) of ZnS films is determined using the following relations [47].

$$\delta = \frac{1}{D} \quad (9)$$

The XRD parameters for the most intense peak (111) are shown in Table 1

TABLE 1. Structural parameters of ZnS thin films deposited at different deposition times obtained from (111) peaks.

ZnS thin films	Deposition time (min)	2θ (degree)	FWHM (β) x 10^{-3} (radian)	D (nm)	δ(x10^{15}) (lines/m^2)	ε(x 10^{-3})
As-deposited	30	28.75	10.21	14.66	4.65	2.47
As-deposited	60	28.75	4.11	36.42	0.75	1.00
Annealed	60	28.74	2.93	51.11	0.38	0.71

The full width at half maximum (FWHM) and crystallite size values have an acceptable connection with the crystallinity. The higher values of FWHM point out the reduction of the crystallinity, whereas the bigger crystallite sizes specify the better crystallinity of the films [48]. From Table 1, the values of the FWHM are found, for the as-deposited films, to decrease with increasing deposition time. The crystallite size is seen to increase from 14.66 to 36.42 nm with increasing deposition time from 30 to 60 min. Dislocation density and microstrain, on the other hand, reduce with increasing deposition time. There is also an observed increase in the crystallite size of the as-deposited film (60 min) after annealing in air at 673 K and this can be attributed to the coalescence of grains, stress/strain reduction, and improvement in the structural properties of the thin film layers [49]. Reduction in the dislocation density and microstrain in the ZnS films was also noticed after annealing. This observation suggests an enhancement in the film's crystallinity and a reduction in structural deformations and disorders [32].

3.6 Optical Characteristics

Transmission spectra for the prepared ZnS thin films, before and after annealing at 673 K and measured within the wavelength ranging from 300 to 1000 nm, are shown in Figs. 6(a) and 6(b). From Fig. 6(a), the observed maximum transmittance values at the visible region for the films deposited for 30, 45, and 60 min are 82.1, 68.0, and 61.5%, respectively. These values are comparable to the previously reported values by some authors. For instance, maximum transmissions of 80%, 77%, and 65% for as-deposited ZnS thin films prepared by CBD at varying concentrations were reported by Manjulavalli and Kannan [28]. In this case, the films' thickness varies between 308 and 397 nm as the concentration increases. It can be observed from this study that the percentage transmittance decreases with increasing deposition time for the as-deposited as well as the annealed films, and this may be attributed to an increase in thickness as the deposition time increases. From Fig. 6(b), it is clear that annealing the ZnS films increases their optical transmittance. This increase is clearly shown in Fig. 6(b) (inset) for the film deposited for 30 min. The annealed film shows a maximum transmittance of 89.2% in the visible region, as compared to the as-deposited film deposited for the same time (30 min), which gives a maximum transmittance value of 82.1%. This increase could be attributed to the rearrangement and decrease of the film's defects [50]. Bashar *et al*. [46] found a maximum average transmittance of about 84% in the visible region for sputtered ZnS thin films annealed at 673 K. It is essential for a buffer or window layer to be highly transparent, allowing light to pass through to the absorber layer [51]. Therefore, in this study, the prepared ZnS thin film shows high transmittance and can be applied as a buffer layer for thin-film solar cells.

The absorbance (A) of the thin films was calculated from percentage transmittance (%T) by using the relation [52]:

$$A = \log\left(\frac{100}{\%\,T}\right) \quad (10)$$

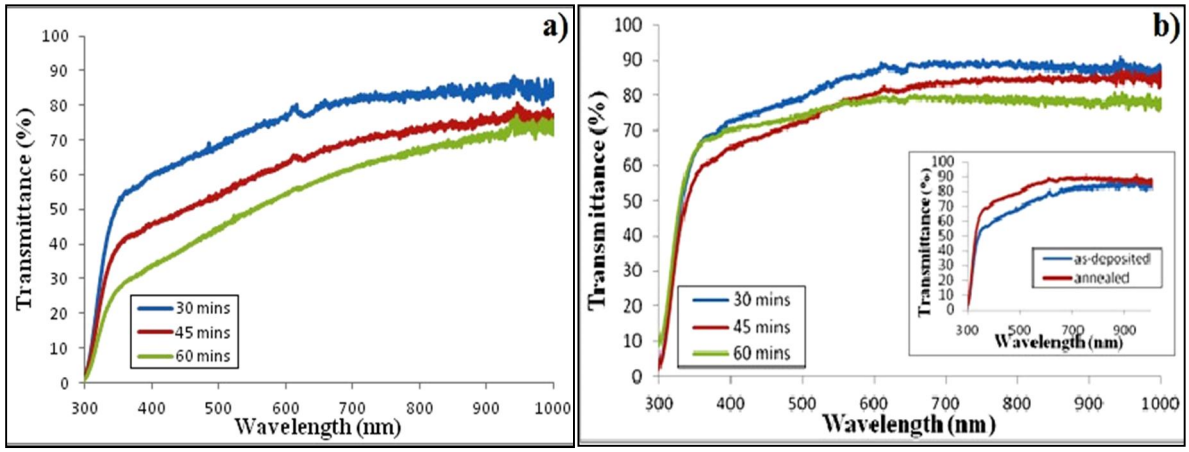

FIG. 6. Transmittance spectra for (a) as-deposited and (b) annealed ZnS thin films deposited for different time periods. Inset: Transmittance spectra for as-deposited and annealed ZnS thin films for 30 min deposition time.

Figs. 7(a) and 7(b) show the optical absorption spectra for as-deposited and annealed ZnS films measured in the spectral range of 300-1000 nm. It is clear from the figures that maximum absorption is observed in the short wavelength region (UV region) and then decreases with increasing photon wavelength within the spectral range. The figure also shows that the percentage absorption increases with increasing deposition times for the as-deposited as well as the annealed films. From the figure, the values of absorption for the annealed films are observed to be lower than that of the as-deposited films, which suggests that post-annealing treatment reduces the absorption of the films (inset). Similar behavior has been observed by Abduljabbar [53], who suggested that the lowering of the percentage absorption may be because the annealed films have higher values of transmittance.

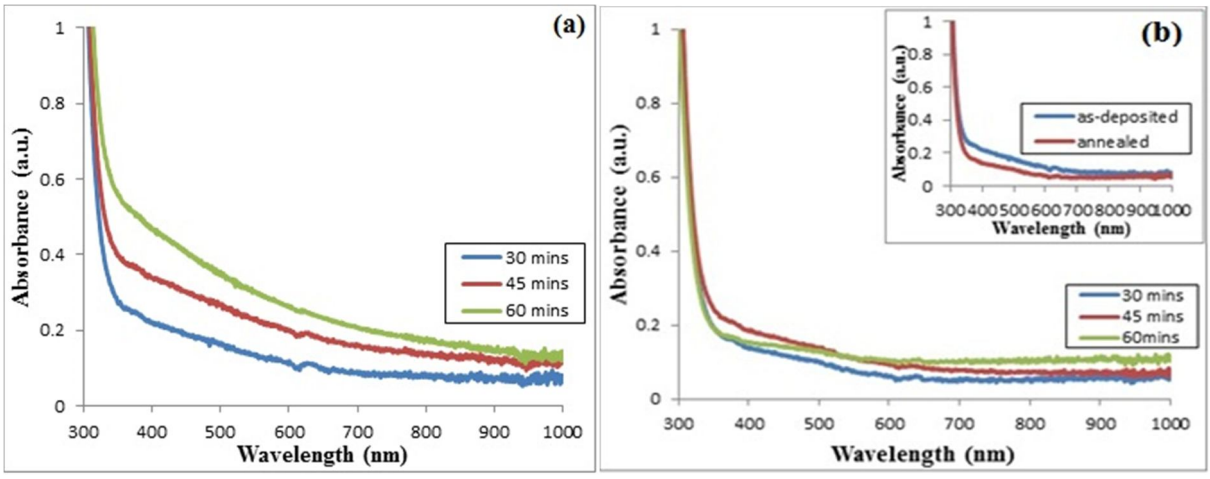

FIG.7. Absorbance spectra for (a) as-deposited and (b) annealed ZnS thin films deposited for different time periods.

The reflectance (% R) was calculated from the absorbance (% A) and transmittance (% T) using the following relation [18]:

$$R + T + A = 1 \quad (11)$$

The variation of reflectance with photon wavelength for the prepared films, before and after annealing, is represented in Fig. 8. The annealed films' spectra are shown in the figure using dash lines. It is clear from the figure that the percentage reflectance decreases with increasing wavelength. A sharp increase in reflectance is observed at a short wavelength < 350 nm. It can also be seen from the figure that there is a significant increase in the reflectance as the deposition time increases for as-deposited as well as annealed films. It is obvious that annealing treatment on the as-deposited films

causes a reduction in the values of the reflectance as clearly shown in the figure (inset). Similar behaviour has previously been reported by some authors [50].

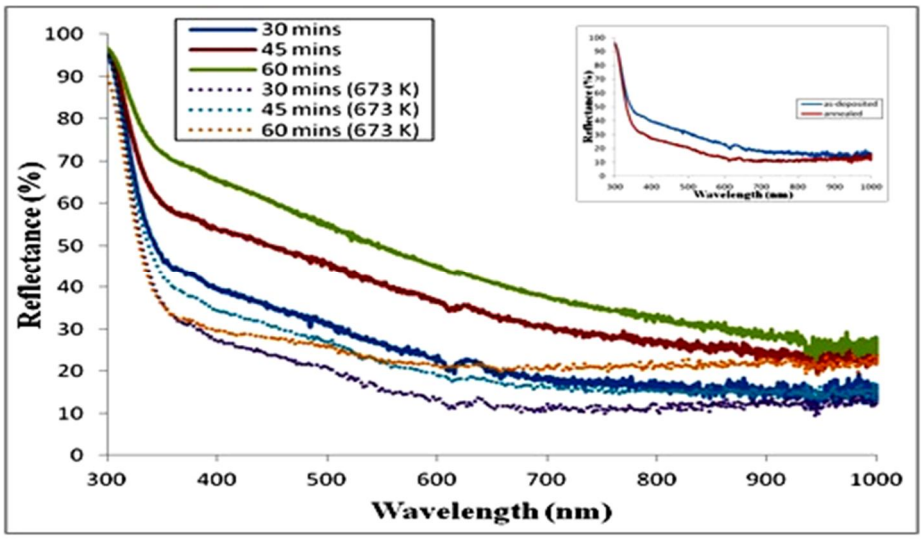

FIG. 8. Reflectance spectra for as-deposited and annealed ZnS thin films deposited for different time periods.

The absorption coefficient (α) which is associated with the strong absorption region of the films was determined from the relation [54]:

$$\alpha = \frac{2.303\ A}{t} \qquad (12)$$

where A is the percentage absorbance and t is the film thickness.

Variation of absorption coefficient with light wavelength is presented in Fig. 9. It has been observed that for all ZnS thin films the absorption coefficient has values, in the order of 10^4 cm^{-1}. From the figure, it is seen that the absorption coefficient reduces with increasing deposition times for all the films. A strong absorption in the ultraviolet region, in contrast with the visible region, is observed for all the ZnS films. A slight reduction in the coefficient of absorption is observed for the annealed film when compared with the as-deposited films. The figure (inset) shows clearly the variation of absorption coefficient with wavelength for the film deposited for 30 min.

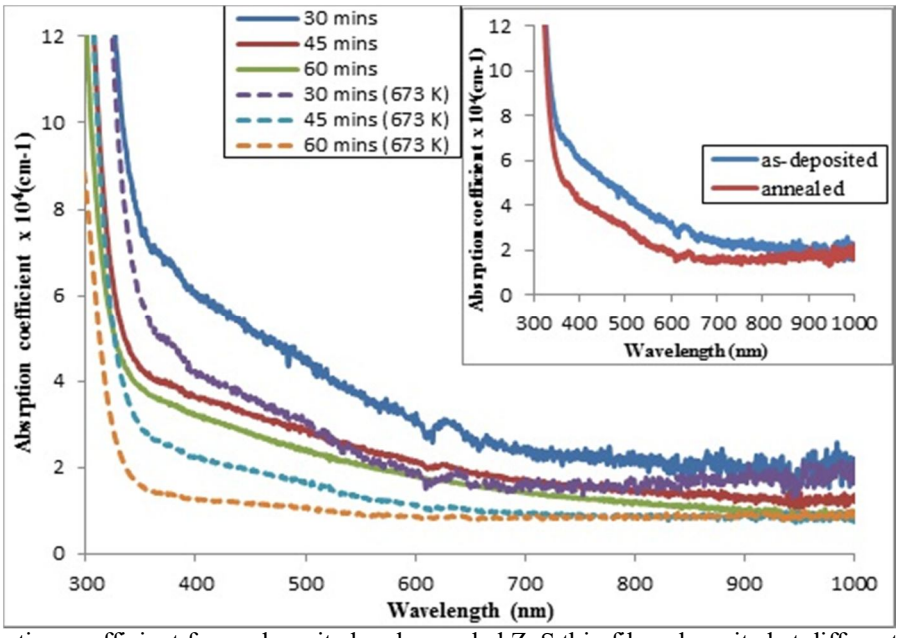

FIG. 9. Absorption coefficient for as-deposited and annealed ZnS thin films deposited at different time periods.

The optical absorption process gives the relationship between the absorption coefficients α and photon energy hν for direct allowed transition as [55]:

$$(\alpha h\nu)^2 = A(h\nu - E_g) \quad (13)$$

where A is a function of the index of refraction and hole/electron effective masses, h is Planck's constant, ν is the light frequency, and E_g is the energy band gap.

The determination of the direct band gap involves extrapolating the linear portion of the plot of $(\alpha h\nu)^2$ against hν to the point where it intersects the energy axis, corresponding to α = 0. The plot of $(\alpha h\nu)^2$ against hν for as-deposited and annealed ZnS thin films deposited for different time periods is shown in Fig. 10.

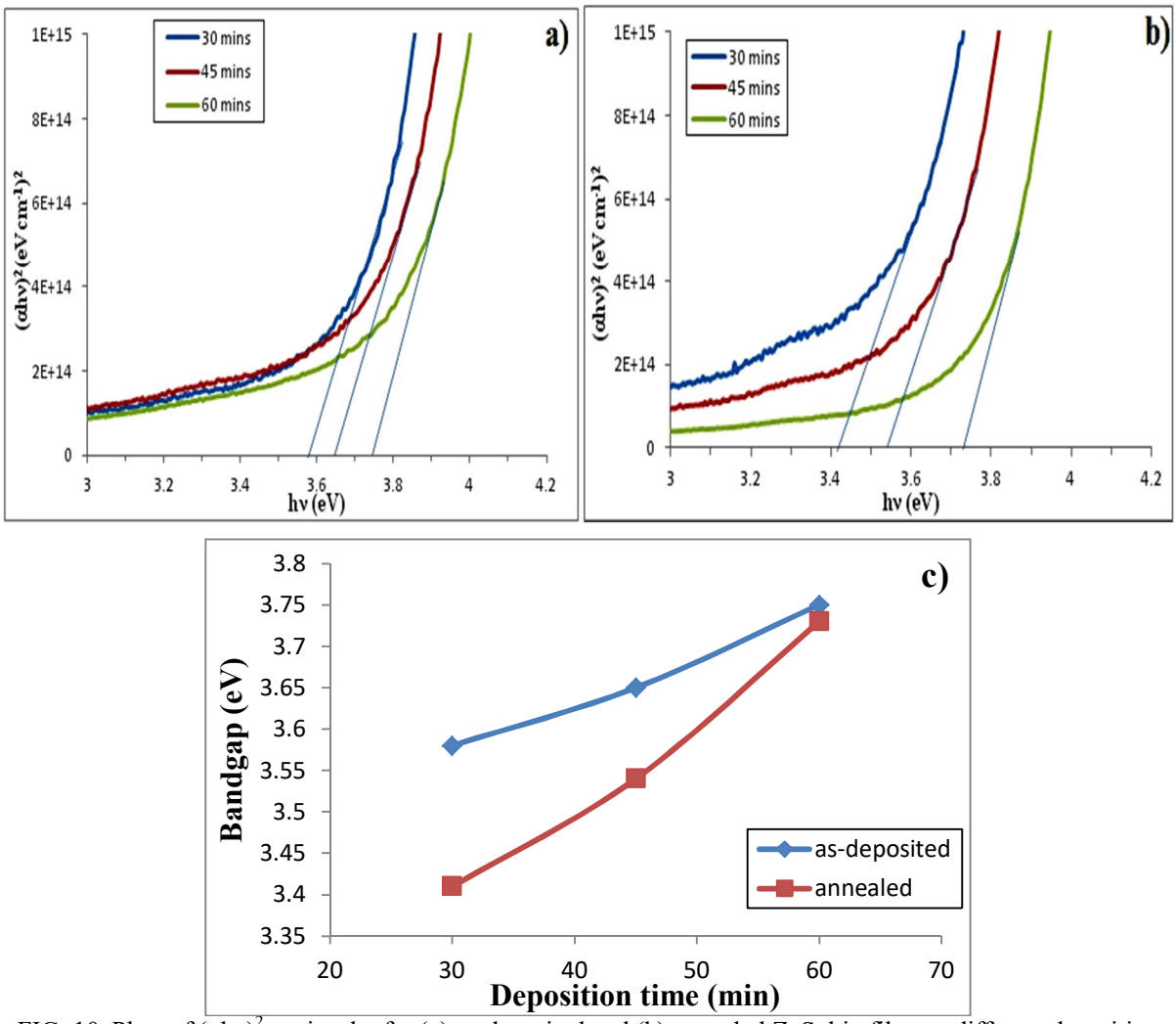

FIG. 10. Plots of $(\alpha h\upsilon)^2$ against hυ for (a) as-deposited and (b) annealed ZnS thin films at different deposition times (c) Variation of energy band gap with deposition temperature.

The values of energy band gaps as obtained from Fig. 10 are presented in Table 2. The table shows that the energy band gap values obtained for the as-deposited ZnS thin films with different deposition time periods vary from 3.58 to 3.75 eV, which are within the band gap value of the bulk ZnS (3.5–3.7 eV). It can be deduced from the table that the energy band gap increases with increasing deposition times for the as-deposited as well as annealed films. The increase in band gap as a result of increasing deposition time can be attributed to a decrease in the disorder in the film [50]. It is observed that the values of energy band gaps for the annealed ZnS films are lower than those of as-deposited ZnS films. The reduction in the films' energy band gap after annealing could be a result of improvement in the crystal structure and change in the sizes of the films' grains. This finding is in good agreement with the reported observations by Ali [56]. The variation of the energy band gap with deposition time for the as-deposited and annealed ZnS films is represented in Fig. 10(c).

TABLE 2. Variation of energy band gap for as-deposited and annealed ZnS thin films deposited for different time periods.

Deposition times (min)	Films thickness (nm)	Energy band gap (eV)	
		as-deposited	annealed
30	72	3.58	3.41
45	125	3.65	3.54
60	150	3.75	3.73

The extinction coefficient (k) gives information about the absorption of a photon in a material medium due to elastic scattering [57] and it is determined from the following equation [58]:

$$k = \frac{\alpha\lambda}{4\pi} \tag{14}$$

where α is the absorption coefficient and λ is the incident photon wavelength

Figure 11 shows the plot of extinction coefficient against wavelength for as-deposited and annealed ZnS thin films at different deposition times. It is clearly seen from the figure that the extinction coefficient decreases with increasing wavelength, as well as with increasing deposition times for both as-deposited and annealed films. The decrease may be attributed to the increase in films' surface roughness due to increasing thickness, which as a result will induce an increase in surface optical scattering. After annealing, the extinction coefficient of films decreases as shown clearly in the figure (inset), representing films deposited for 30 min.

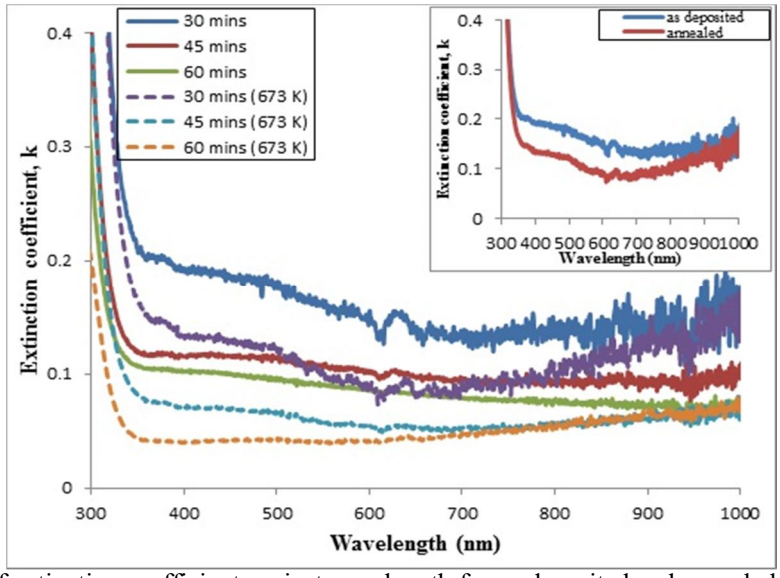

FIG. 11. Plot of extinction coefficient against wavelength for as-deposited and annealed ZnS thin films.

The real and imaginary parts of the dielectric constant of the films were respectively determined by the following relations [59]:

$$\varepsilon_r = n^2 - k^2 \tag{15}$$

and

$$\varepsilon_i = 2nk \tag{16}$$

where n is the refractive index and k is the extinction coefficient.

Figures 12(a) and 12(b) show the dependence of real and imaginary parts of the dielectric constant on photon wavelength for the prepared ZnS thin films. The dielectric constant plot for the annealed ZnS films is indicated by dash lines in the figure. The figure shows that the plot of the real part of the dielectric constant follows the same trend as the transmittance spectra, as its values increase after annealing at 673 K. Contrariwise, the imaginary part follows the same pattern as the absorption coefficient and extinction coefficient and its values decrease after annealing. For each deposition time, the values of the real part are observed to be higher than that of the imaginary part. It is also clear from the figures that an increase in deposition time causes a decrease in the values of both dielectric constants.

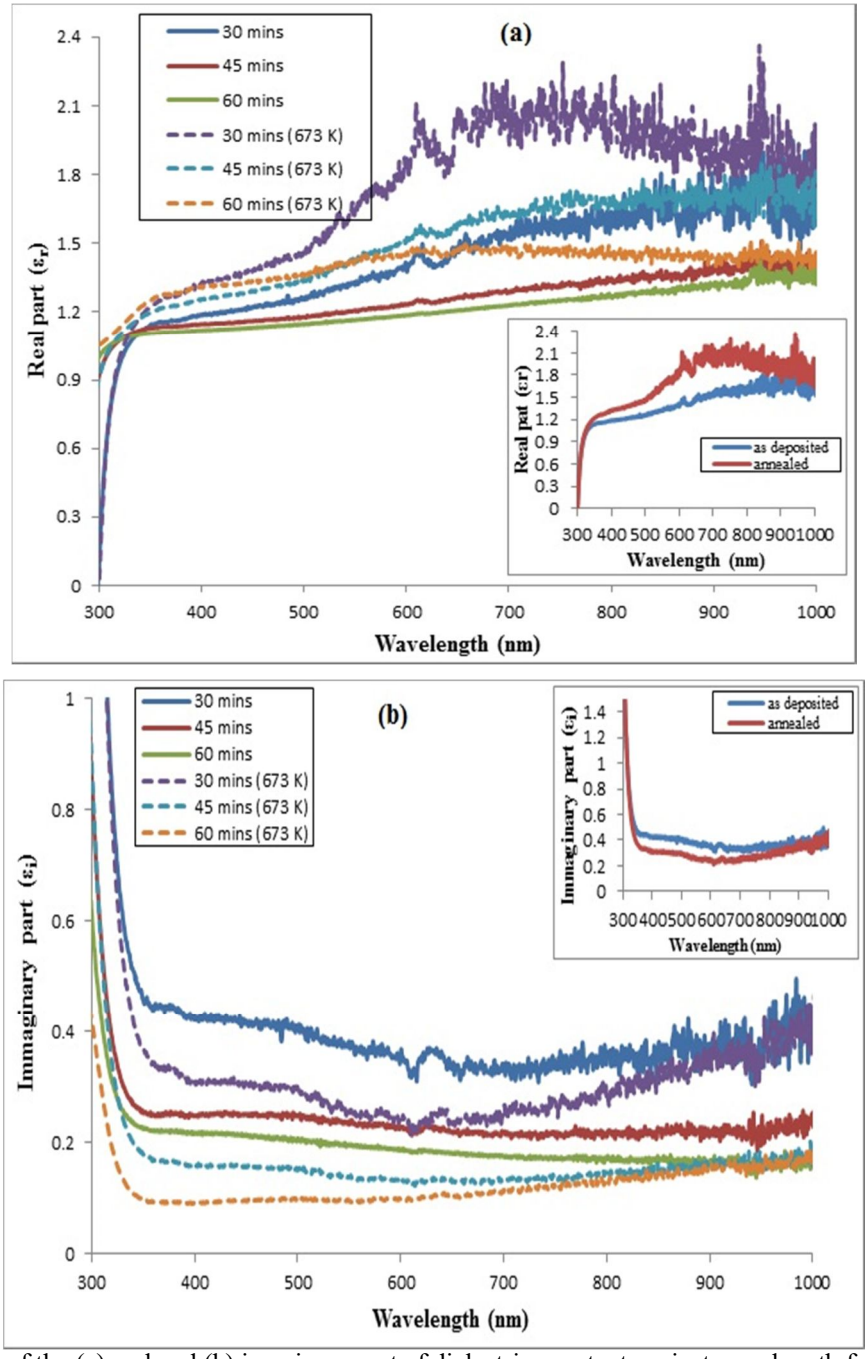

FIG. 12. Plots of the (a) real and (b) imaginary part of dielectric constant against wavelength for as-deposited and annealed ZnS thin films.

The skin depth (χ) is defined as the depth at which the intensity of radiation inside a certain medium reduces to 1/e (about 37%) of the value at the surface and it is determined using the formula [60]:

$$\chi = {}^{1}/_{\alpha} \qquad (17)$$

where α is the absorption coefficient.

Figure 13 shows the plot of skin depth against wavelength in the range of 300-800 nm for as-deposited and annealed ZnS thin films prepared at different deposition times. It can be seen from the figure that the values of the skin depth increase with increasing wavelength. The skin depth also shows an increase with increasing deposition times. A significant increase in skin depth was also noticed after annealing the as-deposited films in air at 673 K. This observation is in good agreement with that reported by Bashar *et al.* [46] for sputtered ZnS thin films deposited at 90 W.

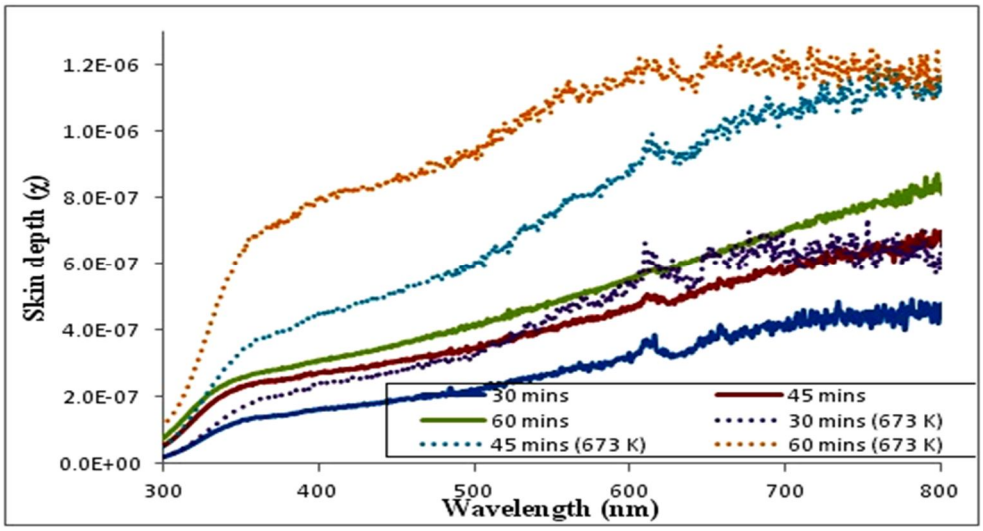

FIG. 13. Plot of Skin depth against wavelength for as-deposited and annealed ZnS.

3.7 FT-IR Analysis

The FT-IR study was used to validate the presence of ZnS and verify the impurities present on the surface of the films. Figure 14 shows the FT-IR spectra for as-deposited and annealed ZnS deposited for 60 min in the range of 4000-400 cm^{-1}. The spectra show the IR absorption due to the various vibration modes. The vibrational assignments as deduced from the spectra are shown in Table 3. The range of broad weak absorption peaks at 3268-3542 cm^{-1} is related to the stretching and bending modes of trace amounts of adsorbed water on the surface of the films [61, 62]. The peak at 2354 cm^{-1} is attributed to the presence of CS_2 or CO molecules [63, 64], while the peak at 1632 cm^{-1} is assigned to the C=O stretching mode [65]. Yet another peak, at 1134 cm^{-1}, is assigned to Zn-OH vibration. Finally, the peaks observed at 514, 604, and 674 cm^{-1} are due to characteristic Zn-S vibration for ZnS thin films, which are in good agreement with the reported results by Jothibas *et al.* [64].

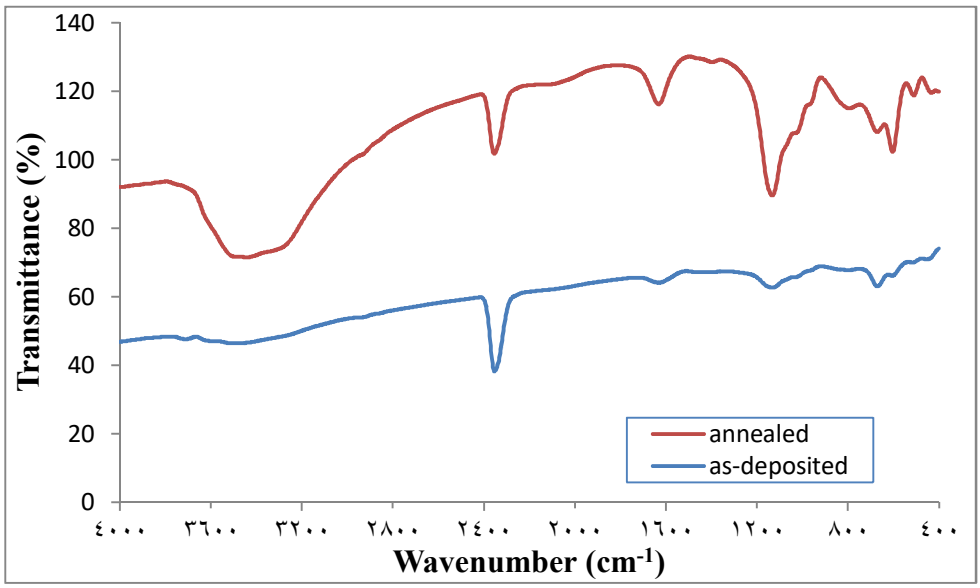

FIG. 14. FT-IR spectra for as-deposited and annealed ZnS deposited for 60 min.

TABLE 3. Vibrational assignments of as-deposited and annealed ZnS thin films.

Wave numbers (cm^{-1})	Assignments
3268-3542	OH stretching
2354	CS_2
1632	C-O stretching
1134	Zn-OH vibration
674	Zn-S band
604	Zn-S band
514	Zn-S band

4. Conclusion

High transparent ZnS thin films of varying thicknesses were prepared by the CBD technique with different deposition durations. The thickness of the prepared ZnS film increases with longer deposition times. X-ray diffraction analysis revealed a cubic structure of the ZnS thin films with diffraction peaks located at 2θ values of 28.75°, 48.05°, and 56.47° and indexed as (111), (220), and (311) reflections. As the deposition time increased, the peaks became more intense and shaper, with one extra weak phase at 2θ values of 33.51°. The parameters of the peaks exhibited further increases after the annealing process. Optical properties of the as-deposited and annealed at 673 K ZnS films were studied. The transmittance is observed to increase with increasing deposition time for the as-deposited as well as the annealed films. The maximum value of the transmittance within the visible range was found to be 82.1% for the as-deposited films and increased to 89.2% after annealing in air at 673 K. The energy band gap expanded as the deposition time increased, with values ranging from 3.58 to 3.75 eV and from 3.41 to 3.73 eV for the as-deposited and annealed films, respectively. After annealing, the energy band decreased. The FT-IR analysis showed peaks at 514, 604, and 674 cm^{-1}, associated with Zn-S vibration. The SEM micrograph displayed a uniformly textured film surface, devoid of voids or pinholes, featuring spherical grains of varying sizes, which disappeared after annealing. The EDX analysis confirmed the presence of both zinc and sulfur in the prepared ZnS film, with evidence of sulfur deficiency. The results of this study clearly indicate that ZnS films can serve effectively as either a buffer or a window layer in solar cells.

References

[1] Mungan, E.S., Wang, Y., Dongaonkar, S., Ely, D.R., Garcia, R.E. and Alam, M.A., IEEE J. Photovolt, 4 (2014) 954.

[2] Arandhara, G., Saikia, P.K. and Bora, J., J. Basic Appl. Eng. Res., 2 (20) (2015) 1761.

[3] Ahn, K., Jeon, J.H., Jeong, S.Y., Kim, J.M., Ahn, H.S., Kim, J.P., Jeong, E.D. and Cho, C.R., Curr. Appl. Phys., 12 (6) (2012) 1465.

[4] Osiele, O.M., J. Appl. Sci., 4 (1) (2001) 1690.

[5] Nasr, T.B., Kamoun, N., Kazari, M. and Bennaceur, R., Thin Solid Films, 500 (2006) 4.

[6] Abdullah, H., Saadah, N. and Shaari, S., World Appl. Sci. J., 19 (8) (2012) 1087.

[7] Nabachandra, A., Singh, L., Singh, R., Nabadwip, S., Singh, S. and Singh, B., Int. J. Lumin. Appl., 3 (1) (2013) 64.

[8] Pathak, C.S., Agarwala, V. and Mandal, M.K., Physica B., 407 (2012) 3309.

[9] Balachander, M., Saroja, M., Venkatalachalam, M. and Shankar, S., Int. J. Innov. Sci. Eng. Technol., 2 (10) (2015) 381.

[10] Hwang, D.H., Ahn, J.H., Hui, K.N., Hui, K.S. and Son, Y.G., Nanoscale Res. Lett., 7 (26) (2012) 1.

[11] Chavhan, S. and Sharma, R., J. Phys. Chem. Solids, 66 (2005) 1721-6.

[12] Nagamani, K., Prathap, P., Lingappa, Y., Miles, R.W. and Reddy, K.T.R., Phys. Procedia, 25 (2012) 137.

[13] Goudarzi, A., Aval, G.M., Sahraei, R. and Ahmadpoor, H., Thin Solid Films, 516 (15) (2008) 4953.

[14] Liu, J., Wei, A. and Zhao, Y., J. Alloy. Compd., 588 (2004) 228.

[15] Oluyamo, S.S. and Abdulsalam, O.A., Niger. J. Pure Appl. Phys., 6 (1) (2015) 33.

[16] Bosco, J.P., Demers, S.B., Kimball, G.M., Lewis, N.S. and Atwater, H.A., J. Appl. Phys., 112 (9) (2012) 093703.

[17] Yano, S., Schroeder, R., Sakai, H. and Ullrich, B., Appl. Phys, 82 (13) (2003) 2026.

[18] Bhalerao, B.A., Lokhande, D.C. and Wagh, G.B., Nanotechnology, 12 (6) (2013) 996.

[19] Khalifa, Z.S. and Mahmoud, S.A., Physica E Low Dimens. Syst. Nanostruct., 91 (2017) 60.

[20] Xu, G., Ji, S., Miao, C., Liu, G. and Ye, C., J. Mater. Chem., 22 (11) (2012) 4890.

[21] Kriisa, M., Kiirber, E., Krunks, M., Mikli, V., Unt, T., Kukk, M. and Mere, A., Thin Solid Films, 555 (2014) 87.

[22] Agawane, G.L., Shin, S.W., Kim, M.S., Suryawanshi, M.P., Gurav, K.V., Moholkar, A.V., Lee, J.Y., Yun, J.H., Patil, P.S. and Kim, J.H., Curr. Appl. Phys., 13 (5) (2013) 850.

[23] O'Brien, P. and McAleese, J., J. Mater. Chem., 8 (11) (1998) 2309.

[24] Mane, R.S. and Lokhande, C.D., Thin Solid Films, 65 (1) (2000) 1.

[25] Allouche, N.K., Nasr, B.T., Kamoun, N.T. and Guasch, C., Mater. Chem. Phys., 123 (2010) 620.

[26] Cotton, F.A. and Wilkinson, G., "Advanced Inorganic Chemistry", 4th Ed., (John Wiley and Sons, New York, 1980).

[27] Shanmugam, N., Cholan, S., Kannadasan, N., Sathishkumar, K., Viruthagiri, G., J. Nanomater., 2013 (2013) 1.

[28] Manjulavalli, T.E. and Kannan, A.G., Int. J. Chemtech. Res., 8 (11) (2015) 396.

[29] Erken, O., Gunes, M., Ozaslan, D. and Gumus, C., Indian J. Pure. Appl. Phys., 55 (2017) 471.

[30] Sathana, V. and Venkatesan, K., Int. J. Chemtech. Res., 12 (4) (2019) 219.

[31] Martin-Varguez, P.E., Ceh, O., Gonzalez-Panzo, I.J., Tec-Yam, S., Patino, R. and Oliva, A.I., Mater. Sci. Eng., 45 (2013) 012025.

[32] Haque, A.M. and Mahalakshmi, S.J., Adv. Phys., 3 (2) (2014) 159.

[33] Shaban, M., Mustafa, M. and Hamdy, H., IOSR J. Appl. Phys., 7 (6) (2015) 19.

[34] Nakada, T., Furumi, K. and Kunioka, A., IEEE Trans. Elec. Dev., 46 (1999) 2093.

[35] Kalyanasundaram, S., Panneerselvam, K. and Kumar Senthil, V., Asia Pac. J. of Res., 1 (8) (2013) 5.

[36] Liang, G., Fan, P., Chen, C., Luo, J., Zhao, J. and Zhang, D., J. Mater. Sci. Mater. Electron., 26 (2015) 2230.

[37] Yu, F., Ou, S., Yao, P., Wu, B. and Wuu, D., J. Nanomater., 6 (2014) 1.

[38] Choudapura, V.H., Kapatkara, S.B. and Rajub, A.B., Acta Chem. IASI, 27 (2) (2019) 287.

[39] Nabiyouni, G., Sahraei, R., Toghiany, M., Ara, M.H.M. and Hedayati, K., Rev. Adv. Mater. Sci., 27 (2011) 52.

[40] Shanmugavadivu, R.A., Yuvaloshini, J. and Ravi, G., Int. J. Semicond. Sci. Tech., 3 (2) (2013) 33.

[41] Metin, H. and Esen, R., Semicond. Sci. Technol., 18 (7) (2003) 647.

[42] Mustafa, G., Chowdhury, M.R.I., Saha, D.K., Hussain, S. and Islam, O., Dhaka Univ. J. Sci., 60 (2) (2012) 283.

[43] Kumar, S., Kumar, S., Sharma, P., Sharma, V. and Katyal, S.C., J. Appl. Phys., 112 (2012) 123512.

[44] Bendjedidi, H., Attaf, A., Saidi, H., Aida, M.S., Semmari, S., Bouhdjar, A. and Benkhetta, Y., J. Semicond., 36 (2015) 12.

[45] Tariq, G.H. and Niaz, N.A., Chalcogenide Lett., 11 (9) (2014) 461.

[46] Bashar, M.S., Matin, R., Sultana, M., Siddika, A., Rahaman, M., Gafur, M.A. and Ahmed, F., J. Theor. Appl. Phys., 14 (2019) 53.

[47] Kathirvel, P., Manoharan, D., Mohan, S.M. and Kumar, S., J. Optoelectron. Biomed. M., 1 (2009) 25.

[48] Islam, M.A., Rahman, K.S., Sobayel, K., Enam, F.M.T., Ali, A.M., Zaman, M., Akhtaruzzaman, Md. and Amin, N., Sol.

Energ. Mat.. Sol. C., 172 (2017) 384.

[49] Salim, H.I., Olusola, O.I., Ojo, A.A., Urasov, K.A., Dergacheva, M.B. and Dharmadasa, I., J. Mater. Sci-Mater. El., 27 (7) (2016) 6786.

[50] Chabou, N., Birouk, B., Aida, M.S. and Raskin, J.P., Mater. Sci. Poland, 37 (3) (2019) 404.

[51] Gratzel, A.M., "Nanocrystalline Injection Solar Cells", (John Wiley and Sons, Chichester, 2006), chapter 9.

[52] Tariq, K.I., Sharif, R., Iqbal, M.M., Faheem, M.B., Kamboh, A. and Bashir, S., Sci. Int. (Lahore), 27 (5) (2015) 4007.

[53] Abduljabbar, L.M., Iraqi J. Laser, 13 (2014) 29.

[54] Abbas, N.K., Abbas, L.K. and Muhameed, S.A., Int. J. Thin Film Sci. Technol., 2 (2) (2013) 127.

[55] Mukherjee, A. and Mitra, P., J. Phys. Sci., 16 (2012) 171.

[56] Ali, M.M., Bas. J. Sci., 33 (1) (2015) 156.

[57] Chander, S., Purohit, A., Lal, C. and Dhaka, M.S., Mater. Chem. Phys., 185 (2017) 202.

[58] Ilican, S., Zor, M., Caglar, Y. and Caglar, M., Opt. Appl., 36 (1) (2006) 29.

[59] Ilican, S., Caglar, M., Caglar, Y., J. Optoelectron. Adv., 9 (5) (2007) 1414.

[60] Khalid, H.A., Int. Lett. Chem. Phys. Astr., 45 (2015) 24.

[61] Wegmuller, F., J. Colloid Interf. Sci., 116 (1987) 312.

[62] Infahsaeng, Y. and Ummartyotin, S., Results Phys., 7 (2017) 1245.

[63] Shanmugam, N., Cholan, S., Kannadasan, N., Sathishkumar, K. and Viruthagiri, G., Acta A Mol. Biomol., 118 (2014) 557.

[64] Jothibas, M., Manoharan, C., Jeyakumar, S.J., Praveen, P., Punithavathy, I.K. and Richard, J.P., Sol, Energy, 159 (2018) 434.

[65] Iranmanesh, P., Saeednia, S. and Nourzpoor, M., Chin. Phys. B., 24 (4) (2015) 046104.